Supply-controlled calcium carbonate dissolution decouples the seasonal dissolved oxygen and pH minima in Chesapeake Bay

Jianzhong Su,[1,2] Wei-Jun Cai,[1*] Jeremy M. Testa,[3] Jean R. Brodeur,[1] Baoshan Chen,[1] K. Michael Scaboo,[1] Ming Li,[4] Chunqi Shen,[2] Margaret Dolan,[1] Yuan-Yuan Xu,[1,5,6] Yafeng Zhang,[7,8] Najid Hussain[1]

[1]School of Marine Science and Policy, University of Delaware, Newark, Delaware

[2]State Key Laboratory of Marine Resources Utilization in South China Sea, Hainan University, Haikou, China

[3]Chesapeake Biological Laboratory, University of Maryland Center for Environmental Science, Maryland

[4]Horn Point Laboratory, University of Maryland Center for Environmental Science, Cambridge, Maryland

[5]Cooperative Institute for Marine and Atmospheric Studies, University of Miami, Miami, Florida

[6]Atlantic Oceanographic and Meteorological Laboratory, National Oceanic and Atmospheric Administration, Miami, Florida

[7]School of Marine Sciences, Sun Yat-Sen University, Zhuhai, Guangdong, China

[8]Eco-Environmental Monitoring and Research Center, Pearl River Valley and South China Sea Ecology and Environment Administration, Guangzhou, Guangdong, China

For publication in ***Limnology and Oceanography***

Abstract

Acidification can present a stress on organisms and habitats in estuaries in addition to hypoxia. Although oxygen and pH decreases are generally coupled due to aerobic respiration, pH dynamics may be more complex given the multiple modes of buffering in the carbonate system. We studied the seasonal cycle of dissolved oxygen (DO), pH, dissolved inorganic carbon, total alkalinity, and calcium ion (Ca^{2+}) along the main channel of Chesapeake Bay from May to October in 2016. Contrary to the expected co-occurrence of seasonal DO and pH declines in subsurface water, we found that the pH decline ended in June while the DO decline continued until August in mid-Chesapeake Bay. We discovered that aerobic respiration was strong from May to August, but carbonate dissolution was minor in May and June and became substantial in August, which buffered further pH declines and caused the seasonal DO and pH minima mismatch. The rate of calcium carbonate ($CaCO_3$) dissolution was not primarily controlled by the saturation state in bottom water, but was instead likely controlled by the supply of $CaCO_3$ particles. The seasonal variability of Ca^{2+} addition in the mid-bay was connected to Ca^{2+} removal in the upper bay, and the timing of high carbonate dissolution coincided with peak seasonal biomass of upper Bay submerged aquatic vegetation. This study suggests a mechanism for a novel decoupling of DO and pH in estuarine waters associated with $CaCO_3$, but future studies are needed to fully investigate the seasonality of physical transport and cycling of $CaCO_3$.

Ocean acidification is a process where oceanic uptake of anthropogenic CO_2 from the atmosphere lowers surface ocean pH and the saturation state of calcium carbonate (Ω) (Gattuso et al. 2015; Feely et al. 2018). In coastal waters, ocean acidification can be enhanced by eutrophication-induced hypoxia, leading to a greater decrease in pH than expected (Cai et al. 2011, 2017). Hypoxia and acidification tend to co-occur in bottom waters, where organic matter respiration consumes oxygen while generating CO_2, and these stresses can interact to threaten

many marine organisms and ecosystems (Fabry et al. 2008; Tomasetti and Gobler 2020). The occurrence of coupled dissolved oxygen (DO) depletion and pH decrease in space and time has been reported in many coastal systems (Cai et al. 2011; Melzner et al. 2013; Wallace et al. 2014). Although aerobic respiration of organic matter and physical processes tend to dominate oxygen dynamics (Fennel and Testa 2018), pH decline is regulated by additional processes that differentially change dissolved inorganic carbon (DIC) and total alkalinity (TA) (Xue and Cai 2020). These processes include air–water CO_2 exchange, carbonate dissolution and formation, and anaerobic respiration in the sediment and overlying deep water (Cai et al. 2017; Su et al. 2020a). Processes that control the carbonate system and their impacts on pH dynamics in the hypoxic zone are poorly quantified in many systems, and improved understanding will allow for new insights on the interactions between acidification and hypoxia, improvement of process-oriented modeling work, and better-constrained future projections under global climate change.

As the largest estuary on the east coast of the United States, Chesapeake Bay suffers from long-term eutrophication, seasonal bottom water hypoxia and anoxia, and enhanced coastal acidification (Hagy et al. 2004; Kemp et al. 2005; Cai et al. 2017). Numerous field surveys and modeling studies have documented the seasonal, inter-annual, and decadal variations of nutrients inputs, oxygen, organic carbon and their associated controls and linkages in Chesapeake Bay (Testa et al. 2018; Shen et al. 2019b; Ni et al. 2020). However, studies focusing on the carbonate system and acidification in Chesapeake Bay are still few, and often limited in spatial and temporal scales. In the mainstem Chesapeake Bay, five recent studies documented substantial seasonal variations in all carbonate system parameters along the salinity gradient (Brodeur et al. 2019; Shen et al. 2019a, 2020; Chen et al. 2020; Friedman et al. 2020). Waldbusser et al. (2011a,b) also found a long-term pH decline in polyhaline surface water, and elucidated that

lower pH could reduce oyster biocalcification rate and increase shell dissolution rate. Clearly, there are strong spatial and temporal patterns in the carbonate system in Chesapeake Bay, but the underlying mechanisms driving these patterns remain poorly understood.

One example of a poorly understood but increasingly recognized driver of estuarine carbonate system dynamics is the balance and dynamic of calcium carbonate ($CaCO_3$) dissolution and formation. Cai et al. (2017) demonstrated that carbonate dissolution could offset a significant proportion of the metabolic CO_2 effect on acidification during the late summer in Chesapeake Bay. To resolve the apparent TA removal in the upper bay and dissolution signal in the mid-bay bottom water, Su et al. (2020a) proposed that $CaCO_3$ solids formed by precipitation and biocalcification within submerged aquatic vegetation (SAV) beds contribute to dissolution in the mid-bay and thus buffer acidification. Najjar et al. (2019) also found a significant TA sink in the low salinity region of the Potomac estuary, but suggested that the TA sink was likely caused by calcification by invasive bivalve *Corbicula fluminea*. Thus, it appears that $CaCO_3$ dynamics exert great influence on the carbonate system of Chesapeake Bay. However, the seasonal patterns of carbonate dissolution and formation and their spatial linkage still remain unclear. Therefore, an observation-based more complete analysis of controls on carbonate system, especially carbonate dissolution and formation, and their impacts on pH dynamics in a seasonal scale in Chesapeake Bay is needed to improve our understanding of interactions between hypoxia and acidification.

The purpose of this study was to investigate spatial and seasonal patterns of DO and pH and their linkages to $CaCO_3$ dynamics in Chesapeake Bay. To do this, we compiled field data from four cruises in May, June, August, and October 2016 (Brodeur et al. 2019; Su et al. 2019, 2020a,b), and applied a two-endmember mixing calculation to differentiate specific

biogeochemical processes controlling carbonate system from physical mixing along the salinity gradient. We then utilized chemical proxies and stoichiometry to quantify the rates of key biogeochemical processes, particularly aerobic respiration, carbonate dissolution and sulfate reduction, and their impacts on DO and pH dynamics over the course of three seasons. Our analysis identified a unique seasonal decoupling of DO and pH that coincided with a seasonal peak in carbonate dissolution, where dissolution appeared to be supply-controlled as $CaCO_3$ was under-saturated in the mid-bay subsurface water during all cruises.

Materials and Methods

Study site

Chesapeake Bay is a large estuary located in the Mid-Atlantic coastal region of the United States (Kemp et al. 2005). A deep and narrow central channel runs through the middle portion of the bay and is flanked by broad, shallow areas. Freshwater input and turbulent mixing drive a two-layer estuarine circulation (Boicourt et al. 1999), resulting in a long water residence time ~180 d in Chesapeake Bay (Du and Shen 2017). Episodic wind events can cause large reductions in stratification and drive lateral circulation between the shoals and the main channel (Goodrich et al. 1987; Xie and Li 2018). The upper bay is well mixed, while most of the central deep channel (as deep as 30 m) is stratified, hosting hypoxic, anoxic, and acidified deep waters.

Sampling and analytical methods

Four cruises were conducted on the R/V *Rachel Carson* during 4–6 May, 6–10 June, 8–12 August, and 10–13 October 2016. At each sampling event, a YSI 6600 was attached to a submersible pump to obtain profiles of temperature, salinity, and DO. Water was pumped to the deck and flowed through a cellulose acetate cartridge filter (pore size 0.45 μm) for sampling.

However, a Cole-Parmer® salinity meter was used to measure salinities in all discrete water samples. The DIC samples were preserved in 250-mL borosilicate glass bottle with 50 μL saturated $HgCl_2$ solution. The TA samples were not poisoned to prevent HgS precipitation and H^+ release in anoxic and low salinity waters (Cai et al. 2017). The DIC samples were measured by a non-dispersive infrared analyzer (AS-C3, Apollo Scitech) within a week (Huang et al. 2012). The TA samples were analyzed by Gran titration in an open-cell setting (AS-ALK2, Apollo Scitech) at a nearby land-based lab within 24 h of collection (Cai et al. 2010a). The precision for DIC and TA was 0.1%. Both DIC and TA measurements were calibrated against certified reference materials.

The pH samples were measured onboard at 25°C within 1 h of collection using an Orion Ross glass electrode, and calibrated with three National Institute of Standards and Technology (NIST) or formerly National Bureau of Standards (NBS) standard buffers (4.01, 7.00, and 10.01). Correcting the junction potential was not attempted in this study (Easley and Byrne 2012; Martell-Bonet and Byrne 2020). Note that pH was also calculated from measured DIC and TA on the NBS scale using a modified version of the CO2SYS program, which included HS^- and NH_3 species in its total alkalinity equation (Xu et al. 2017). Discrete DO samples were measured following Pai et al. (1993) with a precision of ±1 μmol kg^{-1}. Apparent oxygen utilization (AOU) was calculated by subtracting the measured DO from the saturated DO (Pilson 2012). The DO solubility was calculated based on Benson and Krause (1984). Biweekly and monthly DO and pH measurements were also obtained from the Maryland Department of Natural Resources and the Chesapeake Bay Program (http://data.chesapeakebay.net/WaterQuality). We measured Ca^{2+} samples using an auto-titration technique modified from Kanamori and Ikegami (1980) with a precision better than 0.1%. The aragonite saturation state (Ω_{arag}) was derived using measured

Ca^{2+}, calculated CO^{2-}, and aragonite solubility of Mucci (1983). More information can be found in Brodeur et al. (2019) and Su et al. (2020a).

Data analysis based on two-endmember mixing calculation

We first utilized a regional mixing scheme between upper estuarine water and offshore seawater to focus on carbonate dissolution in the mid and lower bay, then used a bay-wide mixing scheme between river water and offshore seawater to examine Ca^{2+} variations over the entire bay, especially in the upper bay. We choose surface water at Sta. CB2.2 as the upper estuarine endmember, because this is a well-mixed station in a narrow section of the upper bay before the bay widens downstream, and there are no adjacent major tributaries. Further analysis showed that the small diel variability of biological activity in the estuarine endmember (<30 μmol kg^{-1}) will not affect our main conclusions.

For the offshore seawater endmember, previous study has developed linear regressions of DIC or TA or Ca^{2+} with salinity in the Mid-Atlantic Bight (Su et al. 2020a). Then, we used the salinity of the ocean endmember (33.618 ± 0.139, mean ± SD of the surface 45 m at a latitude and longitude of 37.13333°N and 73.32533°W on 14 August 2013) in Cai et al. (2017) to derive the offshore endmember values. We assessed the potential impacts of seasonality of DIC, TA, and Ca^{2+} in the offshore seawater endmember on carbonate data analysis, which would not change our main conclusions (see Supplementary Discussion in the Supporting Information).

Compared with the relatively consistent ocean endmember values, large variations exist in the riverine endmember due to the temporal variations of freshwater discharge (Joesoef et al. 2017; Najjar et al. 2019). Previous study has revealed that the riverine carbonate endmembers negatively correlate with river discharge (Su et al. 2020a), thus we derived the riverine endmember of DIC, TA, and Ca^{2+} from the specific discharge rate during each cruise period and

10 d prior (Joesoef et al. 2017). The errors were propagated from the uncertainties of slope and intercept of the linear regression and of the specific freshwater discharge based on Taylor's expression (Taylor 1997). All the endmember values and uncertainties are summarized in Supporting Information Table S2.

Next, we present the details of the two-endmember mixing calculation and how we separate the contributions of different biogeochemical processes to nonconservative behaviors of DIC and TA, and their impacts on pH dynamics. The fractions of the two endmembers were calculated based on the following equations:

$$f_{\mathrm{estu}} = \frac{S_{\mathrm{sw}} - S_{\mathrm{meas}}}{S_{\mathrm{sw}} - S_{\mathrm{estu}}}, \quad (1)$$

$$f_{sw} = 1 - f_{\mathrm{estu}}, \quad (2)$$

where S is the salinity, f is the mixing fraction, the subscripts "estu" and "sw" indicate the estuarine and seawater endmember, and "meas" denotes the measured value at a given location within the estuary. These fractions were then used to predict conservative mixing concentrations (i.e., $[X]_{\mathrm{Mix}}$) of chemical constituents (i.e., DIC, TA, or Ca^{2+}) resulting from two-endmember mixing:

$$[X]_{\mathrm{MIX}} = [X]_{\mathrm{estu}} \times f_{\mathrm{estu}} + [X]_{\mathrm{sw}} \times f_{\mathrm{sw}}. \quad (3)$$

The difference between measured and conservative values is defined as the total nonconservative value of $[X]$ (i.e., $\Delta[X]_{\mathrm{Total}}$):

$$\Delta[X]_{\mathrm{Total}} = [X]_{\mathrm{meas}} - [X]_{\mathrm{MIX}}. \quad (4)$$

The positive or negative $\Delta[X]_{\mathrm{Total}}$ indicates addition or removal of $[X]$ to the water column, which is a composite result driven by multiple biogeochemical processes, such as aerobic respiration (AR) and carbonate dissolution (CD). Then, we subtracted the DIC and TA changes of these two processes from the total nonconservative values (ΔDIC_{Total} and ΔTA_{Total}) to obtain the alterations induced by other processes:

$$\Delta[X]_{\mathrm{Others}} = \Delta[X]_{\mathrm{Total}} - \Delta[X]_{\mathrm{AR}} - \Delta[X]_{\mathrm{CD}}. \quad (5)$$

The definition of "other processes" expands beyond that of the sediment efflux, including anaerobic respiration of organic matter in the sediment and overlying deep water as well as air–water CO_2 exchange. Note that air–water CO_2 exchange affects DIC, but not TA (Wolf-Gladrow et al. 2007). The propagation errors of DIC and TA changes induced by different processes were calculated according to the Taylor's expression (Taylor 1997), and averaged over four cruises.

We calculated pH from DIC and TA in an additive manner, including mixing only (pH_{Mix}), mixing plus aerobic respiration ($pH_{Mix + AR}$), mixing plus aerobic respiration plus carbonate dissolution ($pH_{Mix + AR + CD}$), and all processes involved ($pH_{Mix + AR + CD + Others}$). For simplicity, the simulated pH data are expressed as means (SD) in salinity bins of 1 from 1 to 35. The contribution of a single biogeochemical process to pH dynamics is computed by simple subtraction, although the impact on pH is nonlinear. For instance, the contribution of aerobic respiration (ΔpH_{AR}) equals $pH_{Mix + AR}$ minus pH_{Mix}. Due to the nonlinear nature of pH or the synergistic effect of the two processes on pH, ΔpH_{AR} would be slightly different even for the same AR, depending on the initial pH_{Mix} and contributions from other processes, an effect not explicitly treated here (Cai et al. 2011).

To compute the nonconservative concentration of Ca^{2+} between river water and seawater, the estuarine endmembers (estu) should be substituted with riverine endmembers in Eqs. 1–4. The propagation error of ΔCa^{2+} was calculated in a way similar to Eq. S1 (see Supplementary Discussion in the Supporting Information).

Results and Discussion

Decoupling of the seasonal DO and pH minima

The distributions of DO and pH reflect strong spatial and seasonal variations along the main channel of Chesapeake Bay and a seasonal decoupling of pH and DO minima in the central bottom waters. In May, moderate oxygen depletion and pH declines were found in the bottom water within the northern end of the mid-bay (75–100 km from Susquehanna River), with a minimum DO of 101 μmol kg^{-1} and pH of 7.22 (Fig. 1a,e). In June, DO declined rapidly to as low as 21 μmol kg^{-1} and the below-pycnocline water in the northern mid-bay became hypoxic (DO < 63 μmol kg^{-1}) (Fig. 1b). Low pH water was found not only within the hypoxic zone with a seasonal minimum value of 7.10, but also in the upper bay due to mixing with the relatively low-pH river water, the respiration of terrestrial organic matter, and the depression of photosynthesis by low light availability (Fig. 1f) (Kemp et al. 1997). In August, the bottom hypoxic layer expanded upwards to ~10 m depth and expanded seawards at mid-depths (Fig. 1c). Anoxic water existed at the center of hypoxic zone, while oxygen-deficit water (<94 μmol kg^{-1}) occupied the remaining portion of the deep channel toward the bay mouth. In contrast, the severity of acidification was alleviated in August, resulting in an elevated pH minimum of 7.27 and a landward-retreat of low pH water (Fig. 1g). In October, bottom hypoxia and anoxia disappeared as the water column was reoxygenated (>131 μmol kg^{-1}), and pH

increased (>7.59) as stratification weakened with decreasing water temperature and increasing storms during the fall (Fig. 1d,h).

Considering that our detailed analysis was limited to only four cruises in 2016, we sought to more comprehensively assess seasonal variations in oxygen and pH by examining monthly average bottom DO and pH along the mainstem Bay during 1986–2015. As shown in Fig. 2a, DO was highest in winter and began to decline in spring throughout the Bay. The hypoxic zone (DO < 2 mg L^{-1}) first appeared in the northern end of mid-bay in late spring, then rapidly expanded throughout the mid-bay in early summer and persisted until early autumn. However, the spatial and temporal distributions of bottom pH were decoupled from that of DO (Fig. 2b). Bottom pH showed a general longitudinal pattern that increased seaward. Low pH bottom water (pH < 7.5) first appeared in the southern end of upper bay in early spring, then gradually expanded southward to the southern end of mid-bay in June and July before retreating northward in August and finally disappearing in mid-autumn. The pH minimum zone (pH < 7.2) at the intersection of the upper bay and mid-bay was north of the DO minimum zone. Moreover, the pH minimum zone occurred from April to June, while the DO minimum zone existed during June to August. Taken together, the mismatch of the seasonal DO minimum in August and the seasonal pH minimum in June in mid-bay bottom water was not unique in 2016, but was a persistent summer phenomenon in Chesapeake Bay during the past three decades.

Total nonconservative behavior of DIC and TA

In order to identify and quantify mechanisms causing the mismatch of seasonal DO and pH minima, we first examined the seasonality of distributions of DIC and TA and their key controls, then quantified to what extent different biogeochemical processes affect pH

dynamics. Unlike many coastal systems where DIC and TA are linearly related to salinity, Chesapeake Bay DIC and TA distribution patterns were nonlinearly related to salinity during each of our four cruises in 2016 (Fig. 3), suggesting substantial internal biogeochemical alteration of DIC and TA. Using a two-endmember mixing line between CB2.2 and an offshore seawater endmember, we first examined the spatial and temporal variations of carbonate system properties along the main channel of the mid and lower bay. Generally, total nonconservative DIC and TA (ΔDIC_{Total} and ΔTA_{Total}) were positive and reached peak values in the mid-bay, indicating strong additions of DIC and TA in this region, then decreased to nearly zero in the lower bay (Fig. 4). The peak additions of DIC and TA increased from May (257 and 109 μmol kg^{-1}) to June (341 and 161 μmol kg^{-1}) to August (450 and 348 μmol kg^{-1}), then decreased substantially in October (66 and 73 μmol kg^{-1}). Moreover, the ratio of peak ΔDIC_{Total} to peak ΔTA_{Total} decreased from May (2.4) to June (2.1) to August (1.3) to October (<1), suggesting that there was more DIC generation than TA generation in the spring, which switched to more TA generation than DIC generation in the late summer and fall.

Fraction of the DIC change induced by aerobic respiration

The annual cycle of aerobic and anaerobic respiration, with peak summer rates, is a likely source of the net DIC and TA generation derived from the mixing models (Kemp et al. 1992; Cai et al. 2017). The observed DIC addition induced by aerobic respiration in the mid-bay was quite strong from May to August (up to 151–191 μmol kg^{-1}) as the spring bloom was respired and water temperature increased (Smith and Kemp 1995; Testa and Kemp 2014), then became moderate in October (up to 82 μmol kg^{-1}) (Fig. 5). From May to August, ΔDIC_{AR} increased significantly with depth (Supporting Information Table S4), especially in the area where surface blooms and bottom hypoxia and anoxia occurred. The average ΔDIC_{AR} in mid-

bay bottom water was lower in May (117 ± 20 μmol kg^{-1}, n = 8) compared with June (157 ± 28 μmol kg^{-1}, n = 11) and August (154 ± 31 μmol kg^{-1}, n = 16). However, the computed ΔDIC_{AR} decreased to nearly zero in the bay mouth due to mixing with oxygen-replete offshore seawater. Thus, the seasonality of ΔDIC_{AR} is consistent with a strong annual respiration cycle oper- ating at peak rates within the productive mid-Bay (Smith and Kemp 1995; Cowan and Boynton 1996).

We found that the ΔDIC_{AR} of hypoxic water in June was slightly higher, however, than that in August, decoupling rates of aerobic respiration from temperature. From June to August, the water temperature increased from 17.7°C ± 0.5°C to 26.6°C ± 0.6°C, and salinity increased from 16.9 ± 1.2 to 18.6 ± 1.9 within the hypoxic zone. As oxygen solubility has a negative correlation with temperature and salinity, it decreased significantly from 266 ± 3 to 224 ± 4 μmol kg^{-1}, while the average measured DO decreased less significantly from 42 ± 13 to 19 ± 16 μmol kg^{-1}, resulting in a larger AOU in June (224 ± 15 μmol kg^{-1}) than that in August (205 ± 17 μmol kg^{-1}). Theoretically, warming could accelerate the rates of bacterial growth and organic matter decomposition for a given availability of substrate, leading to higher oxygen consumption rates (Brown et al. 2004). However, the unexpected smaller AOU in August suggests that factors other than temperature dominated the seasonal change of respiration rates from June to August. One possibility is that lower availability of organic substrates in August limits biological respiration rate, as phytoplankton blooms and bottom water chlorophyll *a* and organic carbon accumulation peaks in early and late spring (Testa and Kemp 2014; Testa et al. 2018; Shen et al. 2019b), and is rapidly depleted earlier in the summer (Li et al. 2016; Ni et al. 2020). This is also consistent with previous findings that a reduction in the supply of labial organic matter to sediments slows down the total bottom respiration rate and reduces sediment

ammonium efflux in the late summer in the mid-bay (Kemp et al. 1992; Cowan and Boynton 1996; Boynton and Kemp 2008). However, pH within these hypoxic waters was much lower in June (7.17 ± 0.07) than that in August (7.44 ± 0.13), suggesting that pH was not solely controlled by aerobic respiration but also by other biogeochemical processes.

Fraction of DIC change induced by carbonate dissolution

We computed the addition of Ca^{2+} as a proxy for the rate of carbonate dissolution seasonally, where we found rates to be minor in the mid-bay in May (<98 μmol kg^{-1}) and June (<63 μmol kg^{-1}), but substantial in August (<201 μmol kg^{-1}) before decreasing in October (<122 μmol kg^{-1}) (Fig. 6). In the lower bay, ΔCa^{2+} decreased to nearly zero toward the bay mouth in August (Fig. 6c). In coastal waters, a strong and apparently linear correlation between Ca^{2+} concentration and salinity may lead to a misinterpretation that Ca^{2+} behaves conservatively. This is because that additions of Ca^{2+} (<201 μmol kg^{-1}) are much smaller than the gradient between river water (~600–800 μmol kg^{-1}) and seawater (~10,000 μmol kg^{-1}) concentrations (Fig. 6), and the relatively large uncertainties of Ca^{2+} measurements (i.e., <0.1% or <10 μmol kg^{-1} for seawater analysis) and endmembers make it difficult to discern non-conservative effects in linear mixing models. Fortunately, the composite uncertainty was usually smaller than the non- conservative Ca^{2+} (i.e., ΔCa^{2+}) signal (Fig. 6, Supporting Information Tables S3 and S4), and did not preclude us from reaching a conclusion that carbonate dissolution peaked in August of 2016 and was much higher than other months.

The seasonality in estimated dissolution rates was influenced by wind events. The October cruise began at the height of a strong wind event, when the highest wind speed exceeded more than twice the normal value ~5 m s^{-1}. Strong wind-driven mixing introduced nutrient-replete bottom water to the mid-bay surface water and stimulated phytoplankton

primary production, where oxygen saturation reached up to 162% (Fig. 1d). After the wind event (11–13 October), Ca^{2+} was added (<122 μmol kg^{-1}) in the southern part of mid-bay comparable to other seasons (Fig. 6(d)). In contrast, during wind event (10–11 October), Ca^{2+} was removed (<84 μmol kg^{-1}) in the northern part of mid-bay at Stas. 858, CB4.1, and CB4.2 distinct from other seasons (Fig. 6d). As the underlying mechanism remains unknown, the unexpected removal signals of Ca^{2+} were not included in our data interpretation. During this cruise, ΔCa^{2+} was still positive near the bay mouth (CB7.4 and AO1) in October (Fig. 6d), when a wind event induced strong vertical mixing in the relatively shallow bay mouth.

Other processes contributing to changes of DIC and TA

Other biogeochemical processes can also alter DIC and/or TA, including air–water CO_2 exchange (only DIC) and anaerobic respiration of organic matter in the sediment including the processes of denitrification, MnO_2 and FeOOH reduction, sulfate reduction, and methanogenesis (both DIC and TA) (Cai et al. 2010b). These processes typically serve as sources of DIC and TA to the water column and thus we lump them together as "Others." As shown in Supporting Information Fig. S3, DIC addition induced by other processes (ΔDIC_{Others}) increased somewhat from May (<97 μmol kg^{-1}) to June (<157 μmol kg^{-1}) to August (<176 μmol kg^{-1}) in the mid-bay. In October, ΔDIC_{Others} was negative (removal) in the mid-bay. The magnitude in the surface water was close to that in the bottom water in mid-bay in May and October, but increased with depth in June and August though the increase in August (53 μmol kg^{-1}) is only slightly higher than the average propagation error of ΔDIC_{Others} (44 μmol kg^{-1}). In the lower bay, ΔDIC_{Others} decreased to nearly zero toward the bay mouth in August, while ΔDIC_{Others} decreased to a minimum value (-131 μmol kg^{-1}) at Sta. AO1 near the bay mouth in October.

In the mid-bay deep channel subsurface water (>5 m), a portion of ΔTA_{Others} or/and ΔDIC_{Others} values were negative (generally ΔTA_{Others} > -100 μmol kg^{-1} or/and ΔDIC_{Others} > -50 μmol kg^{-1}) (Fig. 7), indicating sinks for TA and DIC, contrary to our expectations. The discrepancy may mainly result from the large errors of ΔTA_{Others} and ΔDIC_{Others} propagated from all other terms (i.e., "Total," "AR," and "CD"), which could reach up to 86 and 43 μmol kg^{-1}, respectively. Another possible explanation is that strong water column mixing in October potentially oxidized HS^- in bottom water or even sulfide minerals in sediments and largely consumed TA. Finally, atmospheric CO_2 invasion could increase bottom-water DIC by ~20–50 μmol kg^{-1} but has no effect on TA in the mid-bay in the summer (Cai et al. 2017; Shen et al. 2019*a*), which could explain the positive intercept of ΔDIC_{Others} in August (Fig. 7c).

Sulfate reduction is the most important pathway for organic carbon mineralization in mid-bay sediments in warm seasons (Burdige and Homstead 1994; Roden et al. 1995). In the upper few cm of mid-bay sediment, dissolved sulfide was previously not detected during spring and autumn, but accumulated up to 2 mmol L^{-1} during summer anoxia (Roden and Tuttle 1993). The combined effect of sulfate reduction followed by sulfide oxidation (by oxygen) on TA and DIC changes is similar to that of aerobic respiration. In contrast, sulfide can be permanently or temporarily stored in the sediment via formation of metal sulfide. Sulfide storage has a minor or no modification on the TA, DIC, and their ratio produced by sulfate reduction. Thus, the accumulation of metal sulfide in the mid-bay sediment can be a proxy for the lower end of sulfate reduction rate, which indicates that sulfate reduction is sufficient to support the observed DIC and TA efflux from sediment to bottom water (Roden and Tuttle 1993). Our further analysis shows that sulfate reduction followed by sulfide storage could produce 24–216 μmol L^{-1} of DIC

and 27-247 μmol L^{-1} of TA to the water column, which is comparable to the positive values of ΔTA_{Others} and ΔDIC_{Others} in Fig. 7.

To reveal what biogeochemical processes regulate the distributions of ΔTA_{Others} and ΔDIC_{Others} in the deep channel, we compiled the data in the mid-bay subsurface water and examined their ratios (Fig. 7). The ratio of $\Delta TA_{Others}/\Delta DIC_{Others}$ in June (0.93) is close to that of denitrification (0.942) and sulfate reduction (1.142). In the summer, the riverine dissolved nitrogen load is low and hypoxia and anoxia impedes nitrification, so denitrification is limited in the mid-bay primarily due to nitrate limitation (Kemp et al. 1990; Testa et al. 2013; Testa et al. 2018). Therefore, sulfate reduction is the dominant anaerobic respiration process in mid-bay sediment in the summer. However, the ratios of $\Delta TA_{Others}/\Delta DIC_{Others}$ in May (1.83) and October (1.81) reflect a combined effect of sulfate reduction and metal oxide reduction (MnO_2 reduction [4.142], FeOOH reduction [8.142]) in the sediment due to the relatively high DO within the mid-bay water column (Fig. 1). The smaller ratio of $\Delta TA_{Others}/\Delta DIC_{Others}$ in August (1.48) may imply that the relative importance of sulfate reduction increased while metal oxide reduction decreased compared with that in May and October due to low or no DO in the mid-bay bottom water and little nitrate to support denitrification. This is consistent with previous studies finding that sulfate reduction reaches peak value in the mid-bay sediment in the summer (Roden and Tuttle 1993; Roden et al. 1995), and much of the metal oxide reduction is dominated by interaction with sulfide, rather than oxidation of sedimentary OM (Burdige 1993; Lustwerk and Burdige 1993).

Summary of ΔDIC and ΔTA

We averaged the data in the mid-bay subsurface water to quantify the contributions of different biogeochemical processes to the ΔDIC_{Total} and ΔTA_{Total}. For DIC, the contribution of aerobic respiration increased gradually from May to August and then decreased substantially in

October. Although the average AOU in the hypoxic zone was 20 μmol kg^{-1} higher in June than in August, the expanded hypoxic or oxygen-deficit volumes in August resulted in an overall higher ΔDIC_{AR} in the mid-bay subsurface water than in June. Carbonate dissolution was minor in May and June, but produced considerable DIC up to 144 ± 33 μmol kg^{-1} or 45% ± 14% in August, which was even higher than the contribution of aerobic respiration (123 ± 53 μmol kg^{-1} or 35% ± 12%). In October, DIC addition was substantially less. The contribution of other processes increased from May to June, then decreased in August and October. For TA, carbonate dissolution was the most important process contributing to TA addition, reaching a peak value (288 ± 66 μmol kg^{-1} or 106% ± 23%) in August. Generally, other processes played a secondary role in TA dynamics. Moreover, aerobic respiration had a limited effect on TA removal during all cruises.

pH simulation based on the evolutions of DIC and TA

To understand how different biogeochemical processes influence pH in the subsurface water, we simulated the pH dynamics on a regional scale between CB2.2 and offshore seawater based on the evolution of DIC and TA from component processes. Under the scenario of conservative mixing (i.e., no biogeochemical processes), the calculated pH in different seasons is relatively higher and converge in the seawater end, but is relatively lower and diverge in the low salinity region (Fig. 8a). The distribution of pH against salinity nearly overlapped in May and October, but was moderately lower in June and significantly lower in August in the low salinity water (Fig. 8a), which were correlated with seasonal variability of freshwater discharge and riverine DIC and TA (Su et al. 2020a). Under the scenario of conservative mixing plus aerobic respiration, pH slightly decreased in October, moderately decreased in May, and significantly decreased in June and August in the mid-bay subsurface water, because aerobic respiration

produces CO_2 and acid resulting in pH decline (Fig. 8b). In contrast, carbonate dissolution can increase TA, and is proposed as a buffer to neutralize anthropogenic and metabolic CO_2 (Andersson et al. 2005; Cai et al. 2017; Macreadie et al. 2017). Since carbonate dissolution was minor in May and June but significant in August, pH changes associated with carbonate dissolution increased slightly in May and June, but were substantially elevated during August in the mid-bay subsurface water, resulting in a higher pH in August, moderate pH in May, and lowest pH in June under the scenario of conservative mixing plus aerobic respiration plus carbonate dissolution (Fig. 8c). With additional consideration of other processes, pH was still lowest in June, while pH in August was lower than that in October in the mid-bay subsuface water (Fig. 8d).

We use the hypoxic waters in June and August as an example to show how different processes influenced pH dynamics and led to a mismatch of the seasonal DO minimum in June and seasonal pH minimum in August. To do this, we first selected a series of simulated pH values at salinity 17 in June and at salinity 18 in August according to the average salinity of the hypoxic zone during this time. We then set the pH induced only by conservative mixing in June as base point and calculated the contributions of each biogeochemical process to pH changes in June and August, respectively. As shown in Table 1, pH calculated from conservative mixing in August is 0.04 units lower than that in June. Since AOU within the hypoxic zone was higher in June than that in August, the pH decline caused by aerobic respiration is larger in June (0.78) than that in August (0.74). In contrast, carbonate dissolution was minor in June but significant in August, thus the pH increase caused by carbonate dissolution is much smaller in June (0.05) than that in August (0.71). Furthermore, other processes increased pH by 0.07 units in June and decreased pH by 0.31 units in August. The sum of the four processes induced a pH decline of

0.66 units at salinity 17 in June and 0.39 units at salinity 18 in August, relative to the base point at salinity 17 in June (Table 1). Therefore, the mismatch of the seasonal DO minimum (near-anoxia in August) and pH minimum (in June) can be attributed to the increased carbonate dissolution in August.

Table 1. Contributions of each biogeochemical process to pH changes in mid-bay deep channel subsurface water in June and August.

pH Changes	June, S = 17	August, S = 18
ΔpH_{Mix}	0*	-0.04 ± 0.01
ΔpH_{AR}	-0.78 ± 0.20	-0.74 ± 0.18
ΔpH_{CD}	0.05 ± 0.31	0.71 ± 0.24
ΔpH_{Others}	0.07 ± 0.33	-0.31 ± 0.25
Sum	-0.66 ± 0.49	-0.39 ± 0.39

*We set the pH induced only by conservative mixing at salinity 17 in June as a base point.

Supply-controlled $CaCO_3$ dissolution

We next sought to address why carbonate dissolution was minor in May and June, but became substantial in August. We addressed this question by first examining the ambient saturation state of $CaCO_3$ minerals (Ω) in these 3 months. When $\Omega > 1$, $CaCO_3$ precipitation or preservation is thermodynamically favored; when $\Omega = 1$, $CaCO_3$ minerals are in equilibrium with the surrounding water; when $\Omega < 1$, $CaCO_3$ dissolution is favored (Mucci 1983). The saturation state of aragonite (Ω_{arag}) in the mid-bay subsurface water during May, June, and August was less than 1, indicating that most of mid-bay subsurface waters were in carbonate dissolution favorable conditions. Therefore, the stronger carbonate dissolution in August was not caused by passing the tipping point of Ω_{arag} switching from >1 to <1, which occurred as early as May while Ω_{arag} reached its seasonal minimum in June. That leads us to speculate that the seasonal carbonate dissolution pattern was controlled by the supply from an external source of $CaCO_3$ solids.

We next sought to identify sources of $CaCO_3$ production. Following the method in Su et al. (2020a), we used the removal of Ca^{2+} to trace the process of $CaCO_3$ formation along the mainstem Chesapeake Bay. The maximum removal of Ca^{2+} usually occurred in the upper bay and increased from May (126 ± 69 μmol kg^{-1}) to June (224 ± 57 μmol kg^{-1}), reaching peak value in August (393 ± 61 μmol kg^{-1}), and then decreased in October (315 ± 63 μmol kg^{-1}) (Fig. 9). As we did not consider an additional river endmember in the Potomac River though it has higher carbonate concentrations and contributes 19% of the annual freshwater input to Chesapeake Bay, our estimates of upper estuarine removals of Ca^{2+}, TA, and DIC are on the conservative side.

The seasonal pattern of Ca^{2+} removal (or $CaCO_3$ formation) in the upper Bay generally coincides with the seasonal cycle of aboveground biomass of SAV in Chesapeake Bay (Moore et al. 2000; Gurbisz et al. 2017), which begins to increase in late spring, reaches a growth peak in the late summer, and declines in the fall, making SAV-driven $CaCO_3$ formation a strong candidate process for $CaCO_3$ sources in Chesapeake Bay. However, Najjar et al. (2019) suggested that bivalve calcification was more explanatory than SAV coverage to interpret a significant TA sink in the low salinity zone of Potomac River Estuary, one of the main tributaries in Chesapeake Bay. It is clear that both abiotic precipitation and the activity of marine calcifiers (e.g., SAV leaves, epiphytes, bivalves) can contribute to sinks of Ca^{2+} and TA in low-salinity waters, but how the $CaCO_3$ solids can be transported downstream and support further carbonate dissolution in the mid-bay subsurface water needs additional explanation. The numerical model simulation in Su et al. (2020a) showed that fine particles with diameters of 2 and 8 μm could reach the mid bay within 10 d and have impacts on the mid and lower bay, while those with a diameter of 20 μm were mostly trapped in the upper bay during the entire summer. Therefore, bivalve shells are much less likely than small $CaCO_3$ particles to be transported long distances to

support dissolution elsewhere, as we observed in the mainstem Chesapeake Bay. Thus, further research is needed to quantify the controls on and alternative sources of $CaCO_3$ formation in Chesapeake Bay and other estuaries, as well as the particle transport mechanisms in the longitudinal and lateral dimensions that distribute $CaCO_3$ generated in low salinity waters. Furthermore, the role of this $CaCO_3$ cycling along the Bay axis and the seasonality of its influence on the status of Chesapeake Bay as a CO_2 source or sink also deserve more research (*see* Supplementary Discussion in the Supporting Information).

Summary and Conclusions

We are the first to report the mismatch of seasonal DO and pH minima in Chesapeake Bay, which is further confirmed by long-term observation data in bottom water during 1986–2015. Our analysis of seasonal distributions and apparent nonconservative transformation rates of carbonate system properties revealed that the seasonal mismatch between DO and pH in oxygen-deleted bottom waters emerges from supply-controlled carbonate dissolution. Our finding that carbonate dissolution in late summer was not primarily controlled by thermodynamic equilibrium as inferred from the low Ω (< 1) has implications for inferences that $CaCO_3$ unsaturated conditions should be associated with dissolution. Our seasonal analysis reinforces the findings of Su et al. (2020a) that $CaCO_3$ solids formed in productive, low-salinity SAV beds is a potential source of $CaCO_3$ to support mid-Bay dissolution and pH buffering. Here, we further clarify the seasonal picture of the carbonate system to suggest that high dissolution rates are restricted to summer because dissolution is supply limited in other seasons. Our proposed mechanisms may be of general applicability to other estuarine systems where SAV or other upstream subsystems may generate $CaCO_3$ solids and support dissolution and buffer pH in

downstream waters. We believe our study sets the stage for more detailed observational and modeling studies to verify the specific processes involved in the potential estuarine pH buffer.

Acknowledgments

This work was supported by NOAA grant NA15NOS4780190. The data in August 2016 have been deposited in the NCEI Ocean Archive with accession number 0209358. The other data in May, June, and October 2016 are in the process of submitting to NCEI. For Dr. Y-Y. Xu, this research was carried out in part under the auspices of the Cooperative Institute for Marine and Atmospheric Studies (CIMAS), a Cooperative Institute of the University of Miami and the National Oceanic and Atmospheric Administration, cooperative agreement No. NA20OAR4320472. We thank the captain and the crew of R/V *Rachel Carson* for their cooperation during the cruise. We thank Casey Hodgkins for assistance on the fieldwork, Eleri Phillips, Kayla Shraboneau, and Colton Williamson for part of calcium sample analyses. This is UMCES Contribution number 6043 and Chesapeake Biological Laboratory Ref. No. [UMCES] CBL 2022-007.

References

Andersson, A. J., F. T. Mackenzie, and A. Lerman. 2005. Coastal ocean and carbonate systems in the high CO_2 world of the Anthropocene. Am. J. Sci. 305: 875–918. https://doi.org/10.2475/ajs.305.9.875

Benson, B. B., and D. Krause. 1984. The concentration and isotopic fractionation of oxygen dissolved in freshwater and seawater in equilibrium with the atmosphere1. Limnol. Oceanogr. 29: 620–632. https://doi.org/10.4319/lo.1984.29.3.0620

Boicourt, W. C., M. Kuzmi c, and T. S. Hopkins. 1999. The inland sea: Circulation of Chesapeake Bay and the Northern Adriatic, p. 81–129. In T. C. Malone, A. Malej, L. W. Harding Jr., N. Smodlaka, and R. E. Turner (eds.), Ecosystems at the land-sea margin: Drainage basin to coastal sea. American Geophysical Union.

Boynton, W. R., and Kemp, W. M. 2008. Estuaries, p. 809-866. In D.G. Capone, D.A. Bronk, M.R. Mulholland, E.J. Carpenter (eds.), Nitrogen in the marine environment, Academic.

Brodeur, J. R., and others. 2019. Chesapeake Bay inorganic carbon: Spatial distribution and seasonal variability. Front. Mar. Sci. 6: 99. https://doi.org/10.3389/fmars.2019.00099

Brown, J. H., J. F. Gillooly, A. P. Allen, V. M. Savage, and G. B. West. 2004. Toward a metabolic theory of ecology. Ecology 85: 1771–1789. https://doi.org/10.1890/03-9000

Burdige, D. J. 1993. The biogeochemistry of manganese and iron reduction in marine sediments. Earth Sci. Rev. 35: 249–284. https://doi.org/10.1016/0012-8252(93)90040-E

Burdige, D. J., and J. Homstead. 1994. Fluxes of dissolved organic carbon from Chesapeake Bay sediments. Geochim. Cosmochim. Acta 58: 3407–3424. https://doi.org/10.1016/0016-7037(94)90095-7

Cai, W.-J., X. Hu, W.-J. Huang, L.-Q. Jiang, Y. Wang, T.-H. Peng, and X. Zhang. 2010*a*. Alkalinity distribution in the western North Atlantic Ocean margins. J. Geophys. Res. Oceans 115: C08014. https://doi.org/10.1029/2009JC005482

Cai, W.-J., G. W. Luther, J. C. Cornwell, and A. E. Giblin. 2010*b*. Carbon cycling and the coupling between proton and electron transfer reactions in aquatic sediments in Lake Champlain. Aquat. Geochem. 16: 421–446. https://doi.org/10.1007/ s10498-010-9097-9

Cai, W.-J., and others. 2011. Acidification of subsurface coastal waters enhanced by eutrophication. Nat. Geosci. 4: 766–770. https://doi.org/10.1038/NGEO1297

Cai, W.-J., and others. 2017. Redox reactions and weak buffering capacity lead to acidification in the Chesapeake Bay. Nat. Commun. 8: 369. https://doi.org/10.1038/s41467-017-00417-7

Chen, B., W.-J. Cai, J. R. Brodeur, N. Hussain, J. M. Testa, W. Ni, and Q. Li. 2020. Seasonal and spatial variability in surface pCO_2 and air–water CO_2 flux in the Chesapeake Bay. Limnol. Oceanogr. 00: 1-20. https://doi.org/10.1002/lno.11573

Cowan, J. L. W., and W. R. Boynton. 1996. Sediment-water oxygen and nutrient exchanges along the longitudinal axis of Chesapeake Bay: Seasonal patterns, controlling factors and ecological significance. Estuaries 19: 562–580. https://doi.org/10.2307/1352518

Du, J., and J. Shen. 2017. Transport of riverine material from multiple Rivers in the Chesapeake Bay: Important control of estuarine circulation on the material distribution. Eur. J. Vasc. Endovasc. Surg. 122: 2998–3013. https://doi.org/10.1002/2016jg003707

Easley, R. A., and R. H. Byrne. 2012. Spectrophotometric calibration of pH electrodes in seawater using purified m-cresol purple. Environ. Sci. Technol. 46: 5018–5024. https://doi.org/10.1021/es300491s

Fabry, V. J., B. A. Seibel, R. A. Feely, and J. C. Orr. 2008. Impacts of ocean acidification on marine fauna and ecosystem processes. ICES J. Mar. Sci. 65: 414–432. https://doi.org/10.1093/icesjms/fsn048

Feely, R. A., R. R. Okazaki, W.-J. Cai, N. Bednaršek, S. R. Alin, R. H. Byrne, and A. Fassbender. 2018. The combined effects of acidification and hypoxia on pH and aragonite saturation in the coastal waters of the California current ecosys- tem and the northern Gulf of Mexico. Cont. Shelf Res. 152: 50–60. https://doi.org/10.1016/j.csr.2017.11.002

Fennel, K., and J. M. Testa. 2018. Biogeochemical controls on coastal hypoxia. Ann. Rev. Mar. Sci. 11: 4.1–4.26. https://doi.org/10.1146/annurev-marine-010318-095138

Friedman, J. R., E. H. Shadwick, M. A. Friedrichs, R. G. Najjar, O. A. De Meo, F. Da, and J. L. Smith. 2020. Seasonal variability of the CO_2 system in a large coastal plain estuary. J. Geophys. Res. Oceans 125: e2019JC015609. https://doi.org/10.1029/2019JC015609

Gattuso, J.-P., and others. 2015. Contrasting futures for ocean and society from different anthropogenic CO_2 emissions scenarios. Science 349: aac4722. https://doi.org/10.1126/science.aac4722

Goodrich, D. M., W. C. Boicourt, P. Hamilton, and D. W. Pritchard. 1987. Wind-induced destratification in Chesapeake Bay. J. Phys. Oceanogr. 17: 2232–2240. https://doi.org/10.1175/1520-0485(1987)017<2232:widicb>2.0.co;2.

Gurbisz, C., W. M. Kemp, J. C. Cornwell, L. P. Sanford, M. S. Owens, and D. C. Hinkle. 2017. Interactive effects of physical and biogeochemical feedback processes in a large submersed plant bed. Estuar. Coast. 40: 1626–1641. https://doi.org/10.1007/s12237-017-0249-7

Hagy, J. D., W. R. Boynton, C. W. Keefe, and K. V. Wood. 2004. Hypoxia in Chesapeake Bay, 1950–2001: Long-term change in relation to nutrient loading and river flow. Estuaries 27: 634–658. https://doi.org/10.1007/BF02907650

Huang, W. J., Y. Wang, and W. J. Cai. 2012. Assessment of sample storage techniques for total alkalinity and dissolved inorganic carbon in seawater. Limnol. Oceanogr. Methods 10: 711–717. https://doi.org/10.4319/lom.2012.10.711

Joesoef, A., D. L. Kirchman, C. K. Sommerfield, and W.-J. Cai. 2017. Seasonal variability of the inorganic carbon system in a large coastal plain estuary. Biogeosciences 14: 4949– 4963. https://doi.org/10.5194/bg-14-4949-2017

Kanamori, S., and H. Ikegami. 1980. Computer-processed potentiometric titration for the determination of calcium and magnesium in sea water. J. Oceanogr. Soc. Japan 36: 177–184. https://doi.org/10.1007/bf02070330

Kemp, W. M., P. Sampou, J. Caffrey, M. Mayer, K. Henriksen, and W. R. Boynton. 1990. Ammonium recycling versus denitrification in Chesapeake Bay sediments. Limnol. Oceanogr. 35: 1545–1563. https://doi.org/10.4319/lo.1990.35.7.1545

Kemp, W. M., P. A. Sampou, J. Garber, J. Tuttle, and W. R. Boynton. 1992. Seasonal depletion of oxygen from bottom waters of Chesapeake Bay: Roles of benthic and planktonic respiration and physical exchange processes. Mar. Ecol. Prog. Ser. 85: 137–152.

Kemp, W. M., E. M. Smith, M. Marvin-DiPasquale, and W. R. Boynton. 1997. Organic carbon balance and net ecosystem metabolism in Chesapeake Bay. Mar. Ecol. Prog. Ser. 150: 229–248. https://doi.org/10.3354/meps150229

Kemp, W., and others. 2005. Eutrophication of Chesapeake Bay: Historical trends and ecological interactions. Mar. Ecol. Prog. Ser. 303: 1–29. https://doi.org/10.3354/meps303001

Li, M., Y. J. Lee, J. M. Testa, Y. Li, W. Ni, W. M. Kemp, and D. M. Di Toro. 2016. What drives interannual variability of hypoxia in Chesapeake Bay: Climate forcing versus nutrient loading? Geophys. Res. Lett. 43: 2127–2134. https://doi.org/10.1002/2015GL067334

Lustwerk, R. L., and D. J. Burdige. 1993. Iron and manganese reduction in Chesapeake Bay sediments. Trans. Am. Geophys. Union (EOS) 74: 326.

Macreadie, P. I., O. Serrano, D. T. Maher, C. M. Duarte, and J. Beardall. 2017. Addressing calcium carbonate cycling in blue carbon accounting. Limnol. Oceanogr. Lett. 2: 195–201. https://doi.org/10.1002/lol2.10052

Martell-Bonet, L., and R. H. Byrne. 2020. Characterization of the nonlinear salinity dependence of glass pH electrodes: A simplified spectrophotometric calibration procedure for potentiometric seawater pH measurements at 25 C in marine and brackish waters: $0.5 \leq S \leq 36$. Mar Chem 220: 103764. https://doi.org/10.1016/j.marchem.2020.103764

Melzner, F., J. Thomsen, W. Koeve, A. Oschlies, M. A. Gutowska, H. W. Bange, H. P. Hansen, and A. Körtzinger. 2013. Future ocean acidification will be amplified by hypoxia in coastal habitats. Mar. Biol. 160: 1875–1888. https://doi.org/10.1007/s00227-012-1954-1

Moore, K. A., D. J. Wilcox, and R. J. Orth. 2000. Analysis of the abundance of submersed aquatic vegetation communities in the Chesapeake Bay. Estuaries 23: 115– 127. https://doi.org/10.2307/1353229

Mucci, A. 1983. The solubility of calcite and aragonite in seawater at various salinities, temperatures, and one atmosphere total pressure. Am. J. Sci. 283: 780–799. https://doi.org/10.2475/ajs.283.7.780

Najjar, R., and others. 2019. Alkalinity in tidal tributaries of the Chesapeake Bay. J. Geophys. Res. Oceans 125. e2019JC015597. https://doi.org/10.1029/2019JC015597

Ni, W., M. Li, and J. M. Testa. 2020. Discerning effects of warming, sea level rise and nutrient management on long-term hypoxia trends in Chesapeake Bay. Sci. Total Environ. 737: 139717. https://doi.org/10.1016/j.scitotenv.2020.139717

Pai, S.-C., G.-C. Gong, and K.-K. Liu. 1993. Determination of dissolved oxygen in seawater by direct spectrophotometry of total iodine. Mar. Chem. 41: 343–351. https://doi.org/10.1016/0304-4203(93)90266

Pilson, M. E. Q. 2012. An introduction to the chemistry of the sea. 2nd, Cambridge University Press.

Roden, E. E., and J. H. Tuttle. 1993. Inorganic sulfur cycling in mid and lower Chesapeake Bay sediments. Mar. Ecol. Prog. Ser. 93: 101–118. https://doi.org/10.3354/meps093101

Roden, E. E., J. H. Tuttle, W. R. Boynton, and W. M. Kemp. 1995. Carbon cycling in mesohaline Chesapeake Bay sedi- ments 1: POC deposition rates and mineralization pathways. J. Mar. Res. 53: 779–819. https://doi.org/10.1357/0022240953213025

Shen, C., and others. 2019*a*. Controls on carbonate system dynamics in a coastal plain estuary: A modeling study. Eur. J. Vasc. Endovasc. Surg. 124: 61–78. https://doi.org/10.1029/2018jg004802

Shen, C., J. M. Testa, W. Ni, W.-J. Cai, M. Li, and W. M. Kemp. 2019*b*. Ecosystem metabolism and carbon balance in Chesapeake Bay: A 30-year analysis using a coupled hydrodynamic-biogeochemical model. J. Geophys. Res. Oceans 124: 6141–6153. https://doi.org/10.1029/2019jc015296

Shen, C., J. M. Testa, M. Li, and W.-J. Cai. 2020. Understanding anthropogenic impacts on pH and aragonite saturation state in Chesapeake Bay: Insights from a 30-year model study. J. Geophys. Res. Biogeosci. 125: e2019JG005620. https://doi.org/10.1029/2019jg005620

Smith, E. M., and W. M. Kemp. 1995. Seasonal and regional variations in plankton community production and respiration for Chesapeake Bay. Mar. Ecol. Prog. Ser. 116: 217–231.

Su, J., W.-J. Cai, N. Hussain, J. Brodeur, B. Chen, and K. Huang. 2019. Simultaneous determination of dissolved inorganic carbon (DIC) concentration and stable isotope (δ^{13}C-DIC) by cavity ring-down spectroscopy: Application to study carbonate dynamics in the Chesapeake Bay. Mar. Chem. 215: 103689. https://doi.org/10.1016/j.marchem.2019.103689

Su, J., and others. 2020a. Chesapeake Bay acidification buffered by spatially decoupled carbonate mineral cycling. Nat. Geosci. 13: 441–447. https://doi.org/10.1038/s41561-020-0584-3

Su, J., and others. 2020b. Source partitioning of oxygen-consuming organic matter in the hypoxic zone of the Chesapeake Bay. Limnol. Oceanogr. 65: 1801–1817. https://doi.org/10.1002/lno.11419

Taylor, J. R. 1997. Chapter 3. Propagation of Uncertainties, 45–79, Ann McGuire, ed. An introduction to error analysis. 2nd, University Science Books. Sausalito.

Testa, J. M., D. C. Brady, D. M. Di Toro, W. R. Boynton, J. C. Cornwell, and W. M. Kemp. 2013. Sediment flux modeling: Simulating nitrogen, phosphorus, and silica cycles. Estuar. Coast. Shelf Sci. 131: 245–263. https://doi.org/10.1016/j.ecss.2013.06.014

Testa, J. M., and W. M. Kemp. 2014. Spatial and temporal patterns of winter–spring oxygen depletion in Chesapeake Bay bottom water. Estuar. Coast. 37: 1432–1448. https://doi.org/10.1007/s12237-014-9775-8

Testa, J. M., W. M. Kemp, and W. R. Boynton. 2018. Season-specific trends and linkages of nitrogen and oxygen cycles in Chesapeake Bay. Limnol. Oceanogr. 63: 2045–2064. https://doi.org/10.1002/lno.10823

Tomasetti, S. J., and C. J. Gobler. 2020. Dissolved oxygen and pH criteria leave fisheries at risk. Science 368: 372–373. https://doi.org/10.1126/science.aba4896

Waldbusser, G. G., R. A. Steenson, and M. A. Green. 2011*a*. Oyster shell dissolution rates in estuarine waters: Effects of pH and Shell legacy. J. Shellfish. Res. 30: 659–669. https://doi.org/10.2983/035.030.0308

Waldbusser, G. G., E. P. Voigt, H. Bergschneider, M. A. Green, and R. I. E. Newell. 2011b. Biocalcification in the eastern oyster (*Crassostrea virginica*) in relation to long-term trends in Chesapeake Bay pH. Estuar. Coast. 34: 221–231. https://doi.org/10.1007/s12237-010-9307-0

Wallace, R. B., H. Baumann, J. S. Grear, R. C. Aller, and C. J. Gobler. 2014. Coastal ocean acidification: The other eutrophication problem. Estuar. Coast. Shelf Sci. 148: 1–13. https://doi.org/10.1016/j.ecss.2014.05.027

Wolf-Gladrow, D. A., R. E. Zeebe, C. Klaas, A. Körtzinger, and A. G. Dickson. 2007. Total alkalinity: The explicit conserva- tive expression and its application to biogeochemical processes. Mar. Chem. 106: 287–300. https://doi.org/10.1016/j.marchem.2007.01.006

Xie, X., and M. Li. 2018. Effects of wind straining on estuarine stratification: A combined observational and modeling study. J. Geophys. Res. Oceans 123: 2363–2380. https://doi.org/10.1002/2017jc013470

Xu, Y.-Y., D. Pierrot, and W.-J. Cai. 2017. Ocean carbonate system computation for anoxic waters using an updated CO2SYS program. Mar. Chem. 195: 90–93. https://doi.org/10.1016/j.marchem.2017.07.002

Xue, L., and W.-J. Cai. 2020. Total alkalinity minus dissolved inorganic carbon as a proxy for deciphering ocean acidification mechanisms. Mar. Chem. 222: 103791. https://doi.org/10.1016/j.marchem.2020.103791

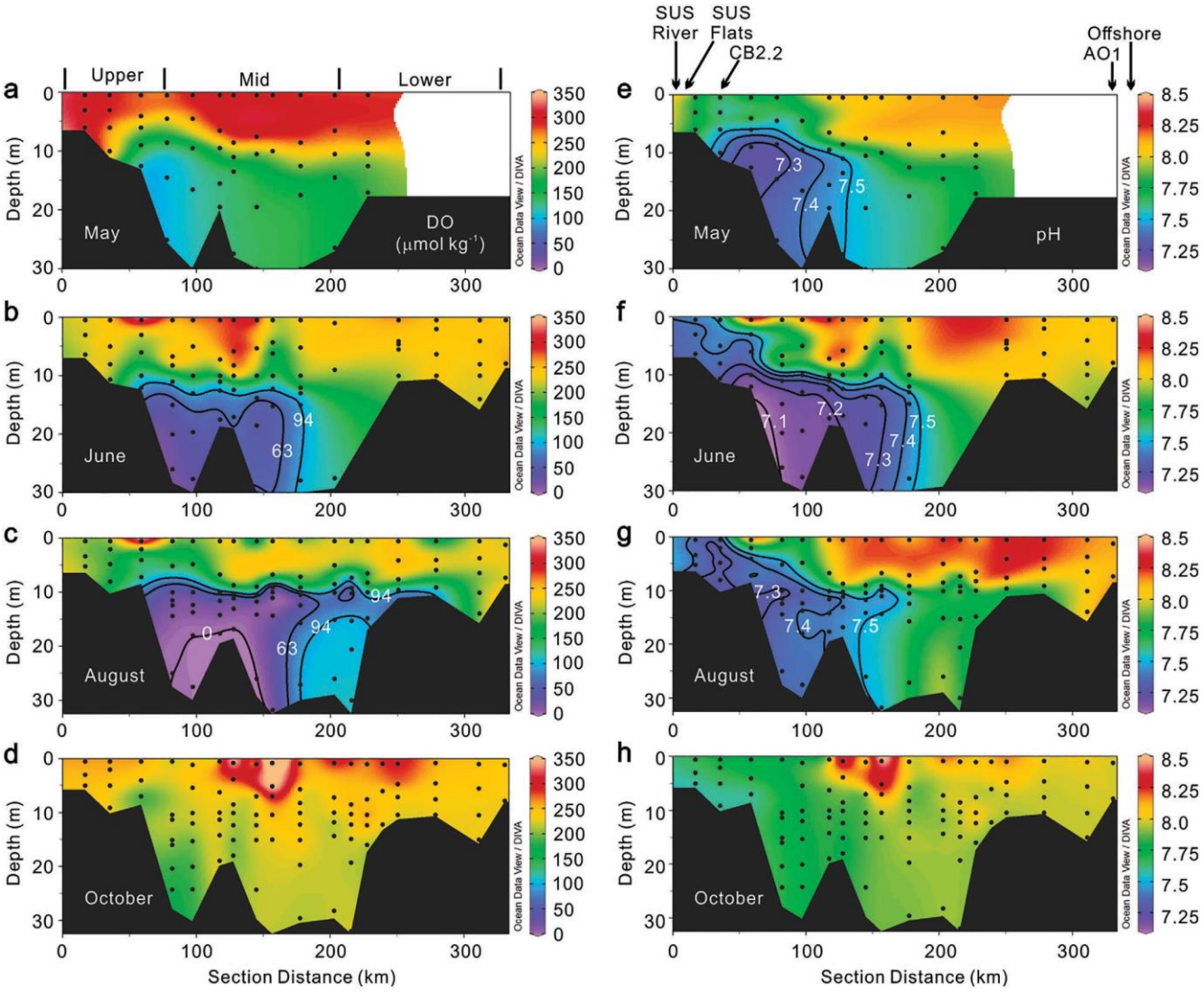

Fig 1. Spatial distributions of dissolved oxygen (DO) and pH along the main channel of Chesapeake Bay in May, June, August, and October 2016. Panels (a)–(d) show DO and contours for anoxia (0 µmol kg^{-1}), hypoxia (< 63 µmol kg^{-1} or roughly <2 mg O_2 L^{-1}), and oxygen-deficit water (<94 µmol kg^{-1} or roughly <3 mg O_2 L^{-1}). Panels (e)–(h) show pH and contours for low pH waters (<7.5). The geological location of this section extends from the Susquehanna River mouth to the bay mouth (AO1). The upper bay (39.0-39.5°N), mid-bay (37.9–39.0°N), and lower bay (37.0–37.9°N) were separated according to Kemp et al. (2005).

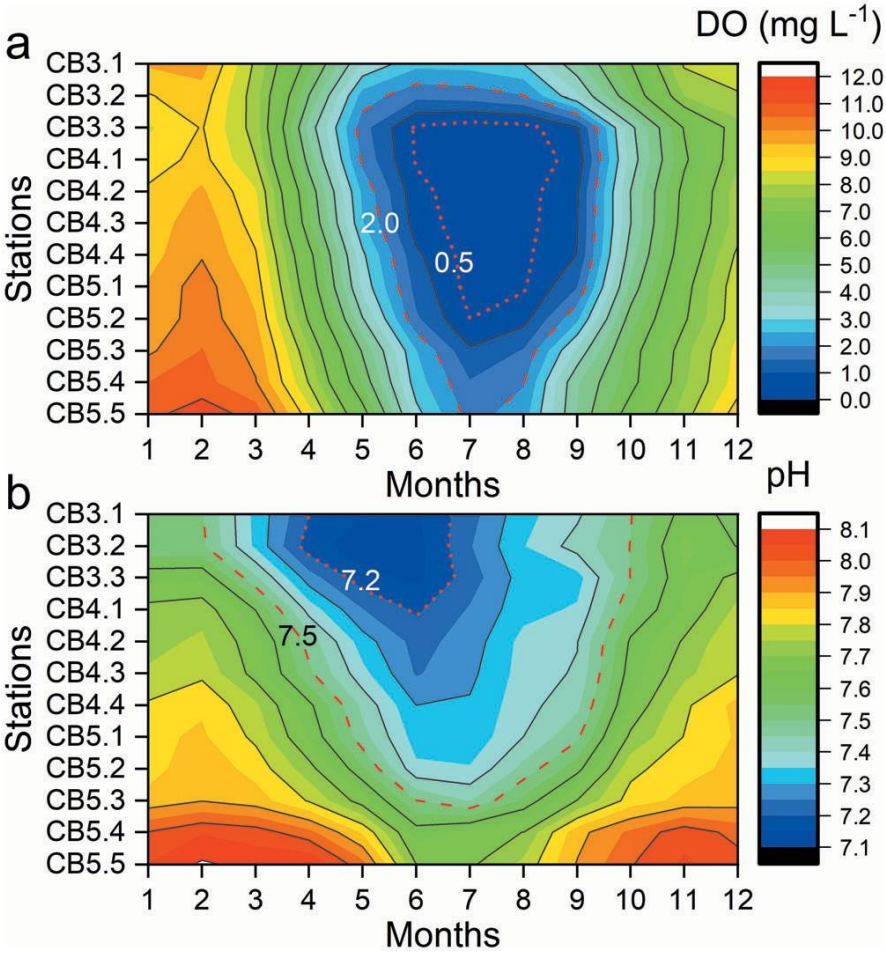

Fig 2. Long-term (1986–2015) monthly average bottom DO and pH along the mainstem bay. The stations were arrayed in an order from upper bay to lower bay, and mid-bay includes Stas. CB3.3 to CB5.3. The red dash lines indicate the hypoxic zone in panel (a) and low pH bottom water in panel (b). The red dot lines indicate the DO minimum zone in panel (a) and pH minimum zone in panel (b). These field data were obtained by the Maryland Department of Natural Resources and the Chesapeake Bay Program (http://data.chesapeakebay.net/WaterQuality).

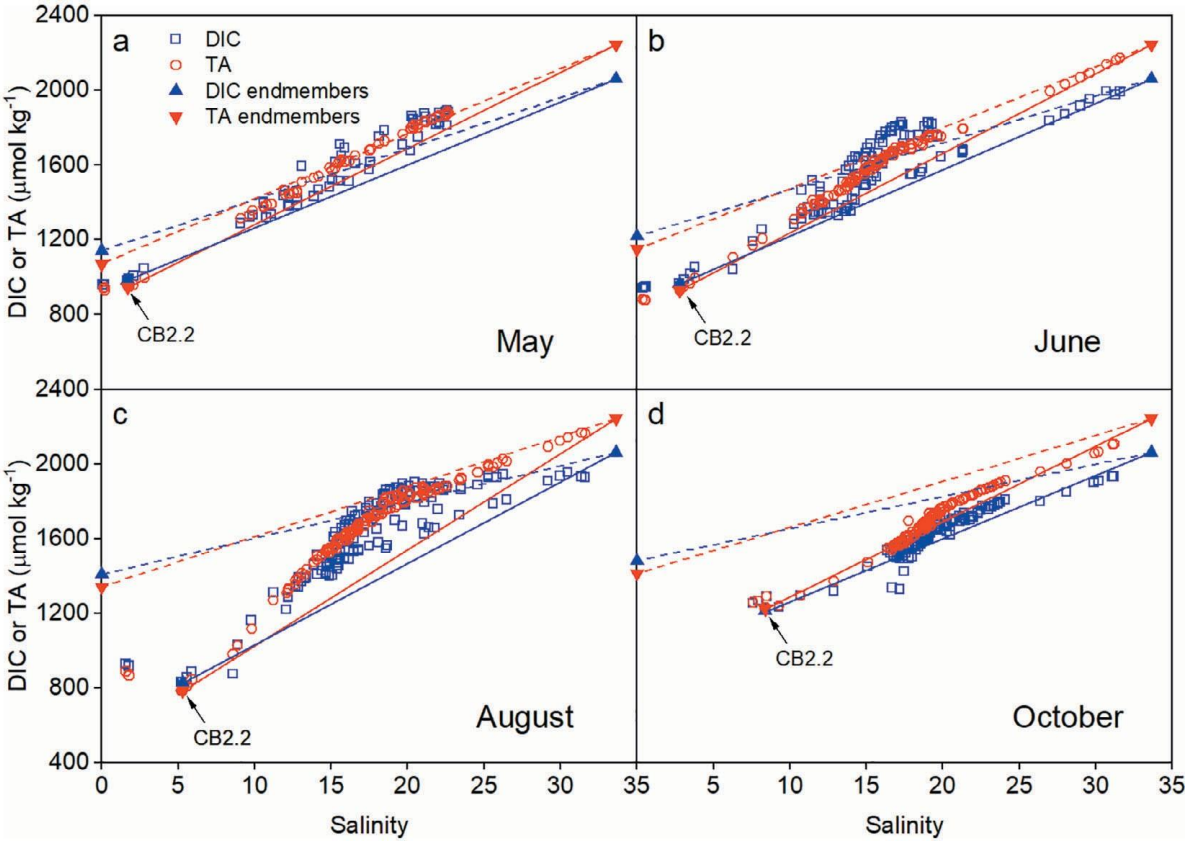

Fig 3. Distributions of dissolved inorganic carbon (DIC) and total alkalinity (TA) against salinity in the mainstem bay in May, June, August, and October 2016. The open circles show the field data, while the filled triangles represent the endmember values. The solid lines indicate the conservative mixing between the estuarine endmember (CB2.2) and the offshore seawater endmember, while the dash lines show the conservative mixing between the riverine endmember and the offshore seawater endmember.

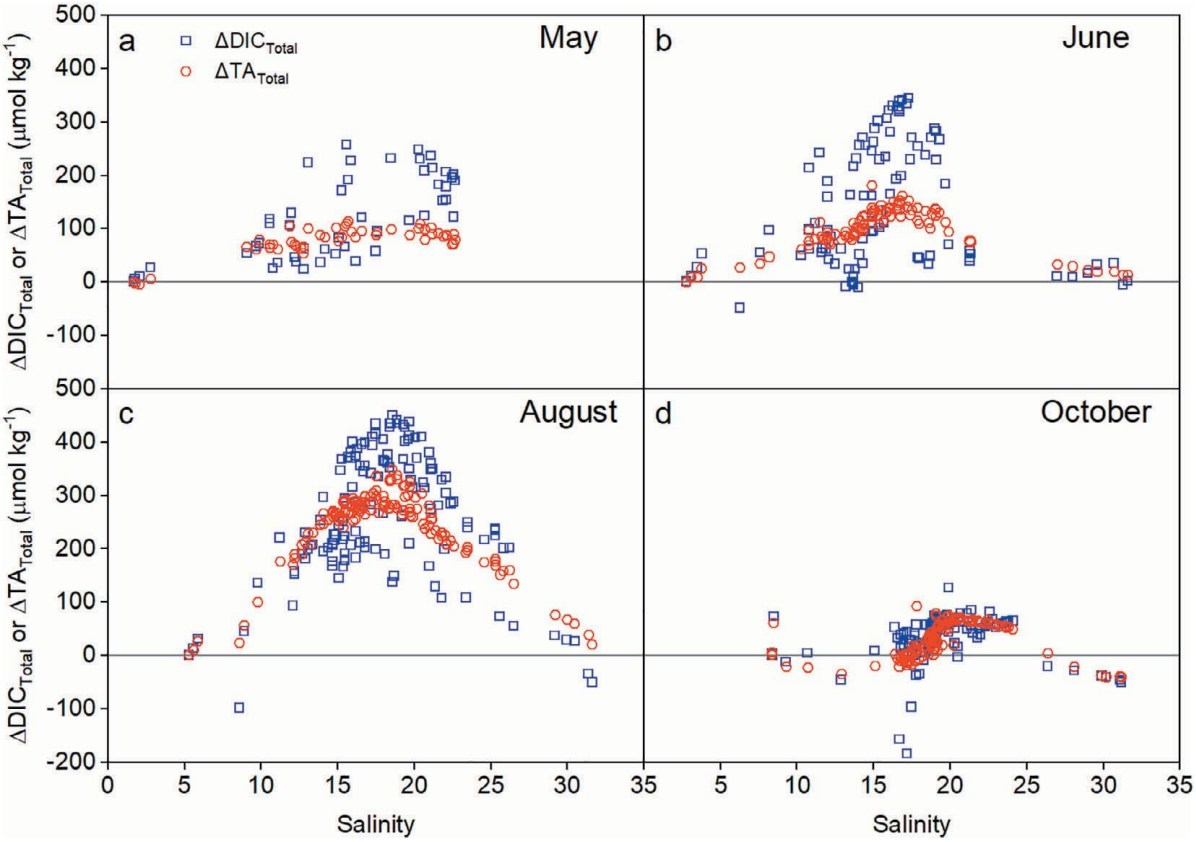

Fig 4. Deviations of dissolved inorganic carbon (DIC) and total alkalinity (TA) from the conservative mixing lines between estuarine and offshore endmembers. These total nonconservative values are a combined effect of multiple biogeochemical processes. Note that a positive (negative) value means chemical addition (removal) to the water column.

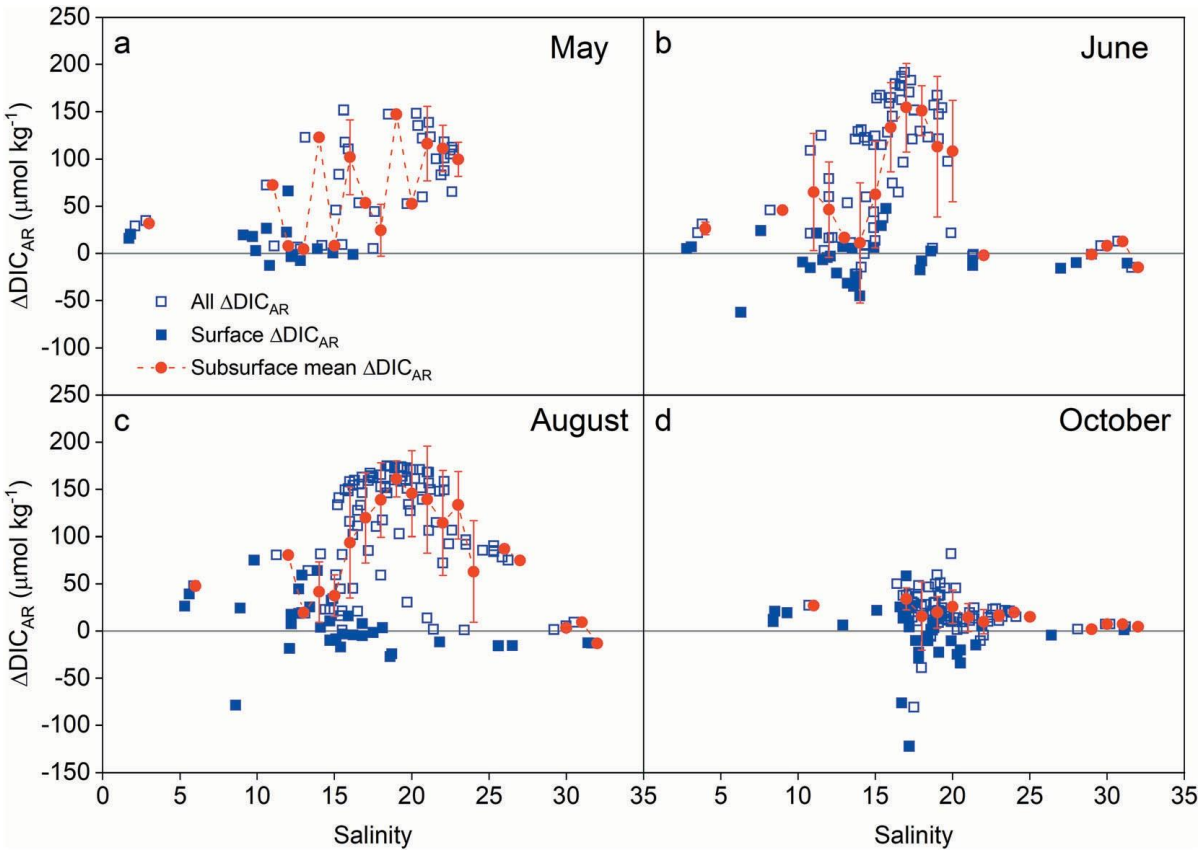

Fig 5. Non-conservative DIC induced by aerobic respiration (AR). Blue squares are field data, while red circles and their error bar represent the value of the mean standard deviation of subsurface water (>5 m) in salinity bins of 1. For example, the field data distributed within salinity 19–20 were represented by the red circle at salinity = 20.

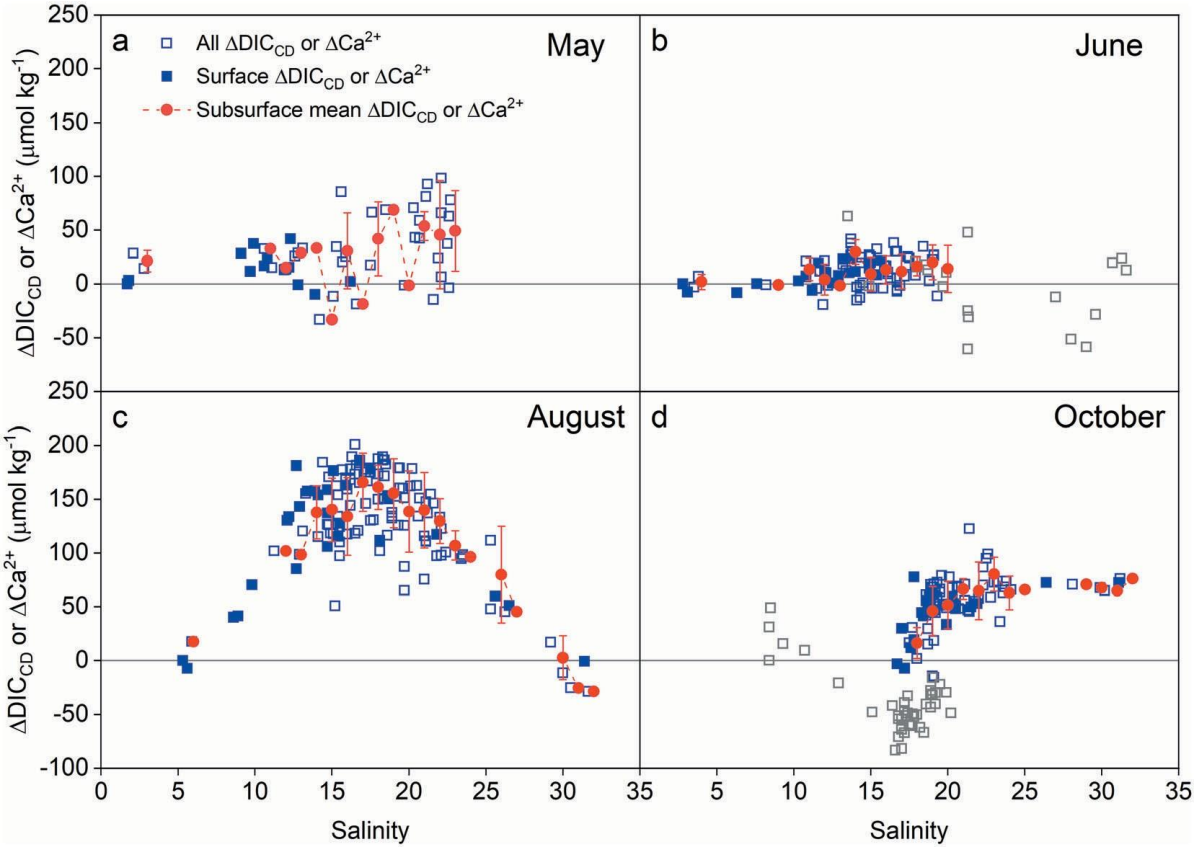

Fig 6. Nonconservative DIC induced by carbonate dissolution (CD). Blue squares are field data, while red circle and its error bar represent the value of mean standard deviation of subsurface water (>5 m) in salinity bins of 1. The gray squares in June (salinity >20) and October (during wind event) were not included in our data interpretation (see Su et al. 2020b and the main text for explanation).

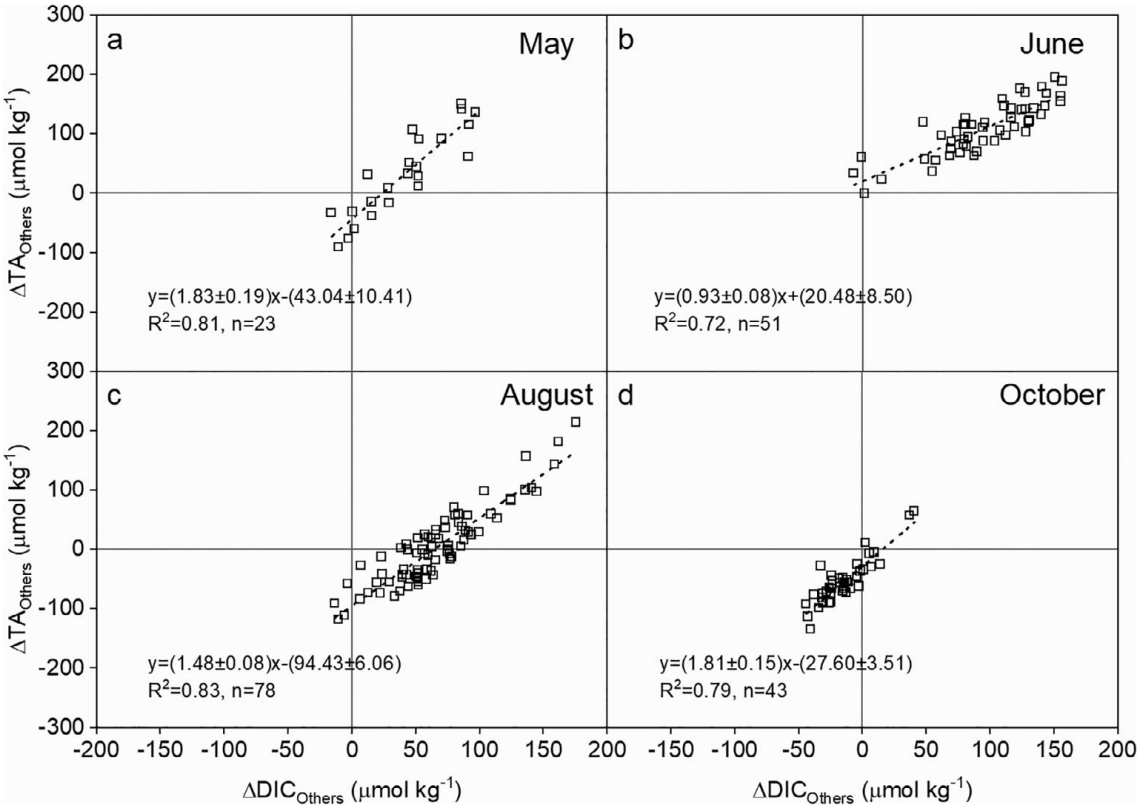

Fig 7. Ratios of nonconservative TA and DIC induced by other processes excluding aerobic respiration and carbonate dissolution in the mid-bay subsurface water.

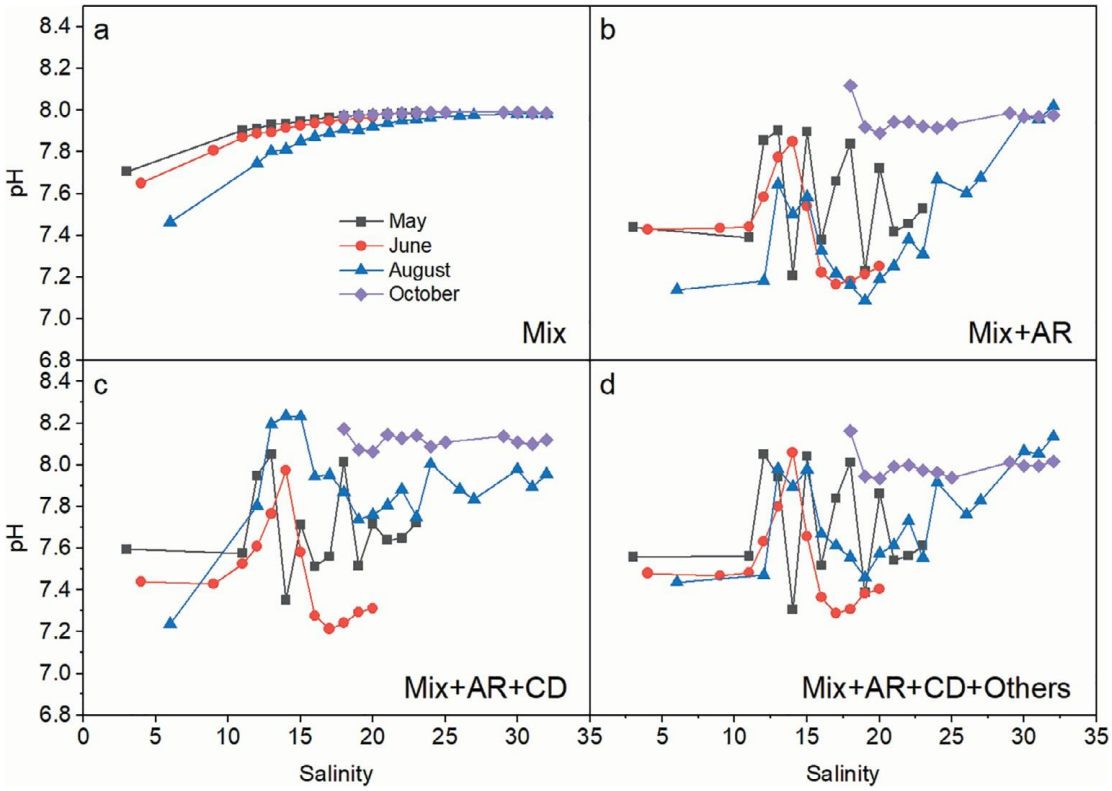

Fig 8. pH simulation in different scenarios. pH was calculated from DIC and TA in an accumulative manner, including mixing only (a), mixing plus aerobic respiration (b), mixing plus aerobic respiration (AR) plus carbonate dissolution (CD) (c), and all processes involved (d).

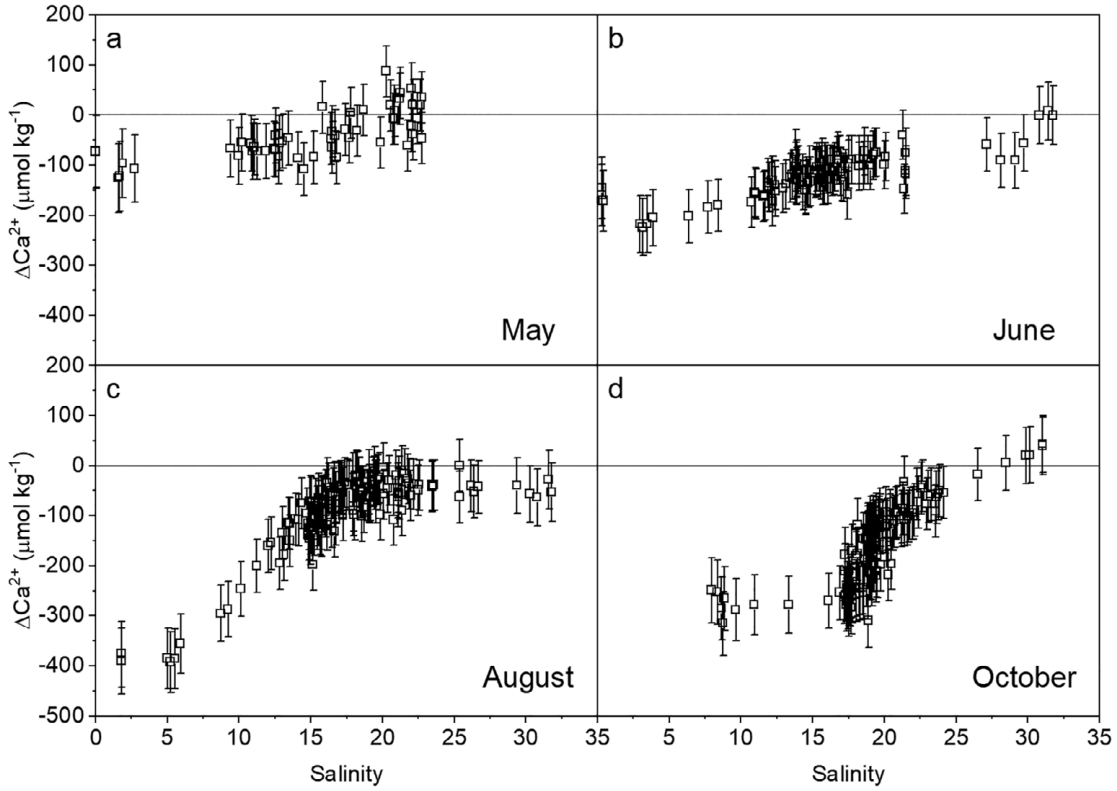

Fig 9. Deviation of calcium ion from conservative mixing between riverine and offshore seawater endmembers. Negative value means removal while positive value means addition of calcium ion across the entire bay. The error bar means propagation error. There is a zero reference line.